Free-Form Deformation as a non-invasive, discrete unfitted domain method: Application to the time-harmonic acoustic response of a saxophone

Marie Jeanneteau, Théo Sentagne, Paul Oumaziz, Robin Bouclier, Jean-Charles Passieux

Computer Methods in Applied Mechanics and Engineering 432 (2024) 117345

Contents lists available at ScienceDirect

Comput. Methods Appl. Mech. Engrg.

journal homepage: www.elsevier.com/locate/cma

Free-Form Deformation as a non-invasive, discrete unfitted domain method: Application to the time-harmonic acoustic response of a saxophone

Marie Jeanneteau [a], Théo Sentagne [a], Paul Oumaziz [a], Robin Bouclier [a,b,c], Jean-Charles Passieux [a,*]

[a] Institut Clement Ader (ICA), Université de Toulouse, CNRS/INSA/UT3/ISAE-SUPAERO/IMT Mines-Albi, Toulouse, France
[b] Institut de Mathématiques de Toulouse (IMT), Université de Toulouse, CNRS/UT1/UT2/UT3/INSA, Toulouse, France
[c] Institut Universitaire de France (IUF), France

ARTICLE INFO

Keywords:
Unfitted discretization
Model order reduction
Splines
Musical acoustics
Finite elements

ABSTRACT

The Finite Element method, widely used for solving Partial Differential Equations, may result in suboptimal computational costs when computing smooth fields within complex geometries. In such situations, IsoGeometric Analysis often offers improved per degree-of-freedom accuracy but building analysis-suitable representation of complex shapes is generally not obvious. This paper introduces a non-invasive, spline-based fictitious domain method using Free-Form Deformation to efficiently solve the Helmholtz equation in complex domains, such as in musical instruments. By immersing a fine FE mesh into a simple B-spline box, the approximation subspace size is significantly reduced without compromising accuracy. Accompanied by specific conditioning treatment, the method not only proves to be efficient, but also robust and easy to implement in existing FE software. Applied to an alto saxophone, the method reduces the number of degrees of freedom by over two orders of magnitude and the computation time by more than one compared to standard FE methods with comparable accuracy when compared to experimental tests.

1. Introduction

In the field of numerical simulation, while pure Artificial Intelligence (AI) and machine learning methods can make accurate and increasingly rapid predictions, the most promising approaches seem to be those that are able to combine the capabilities of AI with physical modeling. The Finite Element (FE) method is one of the most widely used numerical methods for computing the response of physical models by solving Partial Differential Equations (PDEs). The success of this method is mainly due to its ability to solve problems on domains with complex geometry. The idea is to divide the geometry into a finite set of simple geometric elements called "finite elements" and to associate the definition of a functional space with them. To do so, the method is generally based on the concept of isoparametric finite elements [1,2]. This means that the same functional space is used to approximate (i) the geometry and (ii) the unknown field. In certain situations, this property may prove sub-optimal. Indeed, there may be situations in which the geometry is so complex that it requires a very fine mesh, whereas the solution field of the associated PDE may turn out to be much simpler. Using a very fine mesh to represent a complex geometry implies a very large number of unknowns (i.e. Degrees of Freedom, DOF) and potentially over-calculations. This is the case in musical acoustics problems for instance [3].

* Corresponding author.
E-mail address: passieux@insa-toulouse.fr (J.-C. Passieux).

https://doi.org/10.1016/j.cma.2024.117345
Received 14 July 2024; Received in revised form 23 August 2024; Accepted 26 August 2024

The numerical simulation of musical instruments requires high-fidelity models to accurately determine the acoustic pressure field in order to meet the high expectations of professional musicians in terms of tone tuning [3]. This induces a very fine mesh to accurately represent the complex shape of the bore. Surprisingly, even with such complex geometries, the pressure field itself is rather smooth and usually much less complex than what the FE functional space allows to describe. Because of this isoparametric property, such calculations involve excessive computational costs, which can range from a few weeks to months using standard industrial FE tools.

To mitigate this computational cost, IsoGeometric Analysis (IGA) approaches [4,5] for solving PDEs offer several advantages over FE methods. First, they generally present an increased per-DOF accuracy [6–9] thanks to the use of higher-order and smooth bases, such as made of B-spline and Non-Uniform-Rational-B-Spline (NURBS) functions [10,11]. In addition, it is particularly well-suited to wave propagation problems due to the reduction in numerical dispersion and dissipation when exact representation of the domain is possible. In this context, for rather simple geometries that can be accurately represented by a mono- [12] or multi-patch [13,14] mesh, IGA has shown to drastically reduce the computational cost for an equivalent accuracy, when applied to the standard non-convected Helmholtz problem. From an engineering point of view, a good point of IGA is also that efforts have been made to make it compatible with existing FE packages, by relying on the Bézier or Lagrange extraction for instance [15–18]. Furthermore, there are now multiple local refinement techniques that make it a good candidate for acoustic problems [19]. Unfortunately, the Computed Aided Design (CAD) geometries usually considered in engineering applications are often too complex to be suitable for IGA. The practical use of IGA for solving acoustic problems in complex musical instruments remains challenging.

Spline-based fictitious domain methods (also known as *Isogeometric Finite Cell method*, *Unfitted discretization*, *Immersed boundary method*, *CutIGA*, etc.) can avoid this tricky step of building an analysis-suitable spline representation, while keeping a spline-based functional space. The idea is to use an unfitted (usually structured) spline mesh. The problem then shifts to the construction of a fitted quadrature rule [20–22]. This treatment seems particularly well-suited to complex geometries, such as geometries defined by levelsets, that can directly come from digital images [23–25]. However, the fact that these methods are still quite invasive with respect to existing commercial FE software may hinder their widespread industrial adoption.

A few years ago, a method has been proposed, in the field of full-field measurements from digital images, which can actually be seen as a non-invasive fictitious domain technique (see [26] for the introduction and [9] for a formalization). In other words, it can be used easily from existing FE software. The method is based on the concept of Free-Form Deformation (FFD), which was first introduced in [27] in computer graphics. The idea has then been popularized in shape optimization [28–31] as well as in image registration [26,32]. To turn FFD into a non-invasive fictitious domain method, the main idea is to immerse a fitted FE mesh (regardless of its complexity) into a simple bi- or tri-variate (usually B-)spline box, and to relate the nodal FE DOFs of the considered field to another more regular field discretized by the box. The implementation effort is minimal since it is only needed (i) to non-invasively assemble the FE operators using a classic FE library, (ii) to evaluate the spline functions at the nodes of the FE mesh thus building a reduced basis, and (iii) to project the system onto this regular reduced basis [26]. In this respect, the methodology can also be seen as a generalization of the Lagrange extraction to any FE mesh [9]. More recently, similar ideas have been proposed for general PDEs [33], where authors demonstrated additionally relaxation of certain FE meshing constraints within this framework.

In this paper, we propose a FFD-like non-invasive B-spline fictitious domain method, which aims to significantly reduce a frequency-parametrized time-harmonic acoustic problem initially posed over a complex fine fitting FE mesh. More precisely, the developed method allows to project the large FE linear systems onto a more regular, therefore smaller approximation subspace. It is demonstrated that it is possible to reduce the approximation subspace size (and hence the number of DOFs) without compromising accuracy. Thanks to FFD, the approximation subspace of the geometry can be uncoupled from that of the unknown (pressure field here), with non-invasive use of classic isoparametric FE packages. It is also shown how this method works well in the situation of acoustic scattering problems, where most of the operators are constant over the frequency range and can thus be projected once for all frequency steps, in a pre-processing phase. Applied to the analysis of the acoustic response of an alto saxophone over a wide frequency range, the strategy proves to be orders of magnitude faster than classic FE methods with the same mesh.

The paper is organized as follows. In Section 2, the acoustic problem is presented and the proposed FFD acoustic projection is detailed. In this section, the basics on B-spline functions are also briefly recalled. Then, in Section 3, a 2D academic problem whose closed-form is known is first considered to study the ability of the proposed FFD method to provide an accurate pressure field. The computational gain with respect to the classic FE alternative and the robustness of the method regardless of the complexity of the immersion scenario are highlighted. Then, a 3D problem with a complex geometry (including the saxophone body, holes, keyings and outside) is considered to illustrate the performance of the method on a real industrial use case in comparison to experimental results. Finally, Section 4 draws conclusions and outlines future work.

2. The proposed acoustic FFD-based non-invasive fictitious domain method

2.1. Problem statement

Let us consider a time-harmonic acoustic problem defined on a bounded air volume $\Omega \subset \mathbb{R}^d$ ($d = 2$ or 3) characterized by its boundary $S = S_p \cup S_v \cup S_Y$. S_p, S_v and S_Y define a non-overlapping partition of the boundary S where Dirichlet, Neumann and Robin

conditions are applied on, respectively. The acoustic pressure u is solution of the following Helmholtz problem (sign convention for the phase $e^{+j\omega t}$, where $j = \sqrt{-1}$):

$$\begin{cases} \nabla^2 u + k^2 u = 0 & \text{on } \Omega, \\ u = u_0 & \text{on } S_p, \\ v \cdot n = v_0 & \text{on } S_v, \\ v \cdot n + Yu = 0 & \text{on } S_Y, \\ v = -\dfrac{\nabla u}{j\rho\omega} & \text{on } \Omega, \end{cases} \tag{1}$$

where v is the acoustic velocity defined on Ω, $k = \frac{\omega}{c} \in \mathbb{R}$ is the wave number, ω the angular velocity, c speed of sound, ρ the air density, u_0 the pressure prescribed on boundary S_p and v_0 the normal velocity applied on boundary S_v and n the outward unit normal. The viscothermal losses, which is a dissipative phenomena occurring in the acoustic boundary layer, strongly affect the accuracy of the simulations [34]. They are usually modeled by an equivalent admittance Y at the walls of the instrument S_Y in the spirit of Cremer's model [35].

In order to solve numerically this problem, a standard isoparametric FE discretization parametrized by h the characteristic element size, is often used [36]. The computational domain is meshed using finite elements with a sufficiently fine mesh to well represent the geometry. Therefore, the geometry $\mathcal{M}^h(x)$ and the pressure field $u^h(x)$ are approximated as follows:

$$\mathcal{M}^h(x) = \sum_{i=1}^{n_{\text{FE}}} L_i(x) x_i^{\text{FE}} = \mathbf{L}^T(x)\, \mathbf{x}_{\text{FE}} \qquad \text{and} \qquad u^h(x) = \sum_{i=1}^{n_{\text{FE}}} L_i(x) u_i^{\text{FE}} = \mathbf{L}^T(x)\, \mathbf{u}_{\text{FE}} \tag{2}$$

where L_i are FE Lagrange shape functions, x_i^{FE} the coordinates of the FE nodes, u_i^{FE} the nodal pressure values. $\mathbf{L}$, $\mathbf{x}_{\text{FE}}$ and $\mathbf{u}_{\text{FE}}$ are algebraic FE vectors gathering the n_{FE} shape functions, nodal coordinates and nodal values, respectively.

The discretized acoustic pressure $\mathbf{u}_{\text{FE}}$ is solution of the following complex sparse and possibly large-size linear system:

$$\left[\mathbf{K}_{\text{FE}} - \omega^2 \mathbf{M}_{\text{FE}} + \mathbf{\Sigma}_{\text{FE}}(\mathbf{u}_{\text{FE}}) + \mu\, \mathbf{D}_{\text{FE}}\right] \mathbf{u}_{\text{FE}} = \mu\, \mathbf{D}_{\text{FE}}\, \mathbf{u}_{\text{FE}}^d, \tag{3}$$

with $\mathbf{K}_{\text{FE}}$ and $\mathbf{M}_{\text{FE}}$ the standard FE stiffness and mass matrices, respectively. They are sparse, symmetric and possibly large, but since they do not depend on the wave number, they can be assembled once for all frequency step. The damping matrix $\mathbf{\Sigma}_{\text{FE}}$ stands for the dissipative (Robin) conditions at the boundaries. It is naturally far more sparse that the two previous since it concerns only boundary nodes, but it non-linearly depends on the pressure field, and thus the global operator non-affinely depends on the wave number. It is possible to minimize the cost associated to frequency dependence using model order reduction [3,37]. $\mathbf{D}_{\text{FE}}$ is a constant sparse Boolean diagonal matrix used to prescribe Dirichlet boundary conditions with penalization; μ being the penalty factor and $\mathbf{u}_{\text{FE}}^d$ the prescribed pressure values.

The finite element prediction of the acoustic behavior of a musical instrument was shown to be a real challenge in [3], for many reasons: (i) first, given the accuracy required by professional musicians, the FE mesh must be very fine especially at high frequencies and close to the walls to correctly predict the viscothermal losses; (ii) these dissipative effects are commonly modeled, in musical acoustics, using non-linear admittances, such as Cremer's model which depends on the acoustic velocity and thus requires at least solving two large-size linear systems (3). (iii) the accuracy of the simulations also depends on the radiation modeling of the tone holes [38–40], which means that potentially large areas of the surrounding air must be simulated in addition to the bore of the instrument; (iv) the acoustic behavior must be resolved in frequency and given the accuracy of the localization of the peaks, there are usually thousands to tens of thousands frequency steps in the analysis – each step requiring a resolution of one of these large-size non-linear system; (v) to compute the full acoustic response of an instrument approximately 50 different fingerings (i.e. different geometric configurations) must be considered. The acoustic response of one instrument thus requires the solution of almost half million linear systems, each of which of approximately few millions of DOFs. For more details on the implementation, the interested reader is referred to [3]. That is why there is a challenge to further reduce the computational cost of each linear system (3) to make the full simulation of musical instruments compatible with model-based design process.

Another point is that given the very complex shape of musical instruments and especially saxophones, a relatively fine mesh is locally necessary to well describe the geometry. As mentioned in the introduction, because of the isoparametric nature of finite elements, and even if the pressure field itself is rather smooth, the number of DOFs is sometime driven by geometric requirements. Indeed, finite elements lead to a too rich approximation space since it includes C^0 solutions, namely solutions with discontinuous velocities at element edges. Such non-smooth solutions are non-physical because the acoustic field belong to a much more regular space. It is usually not a problem, since the FE approximation space also include more regular solution. But it means that there is room for a reduction in the apparent number of DOFs, without degrading too much the accuracy.

In other words, the idea developed in this paper consists in restricting the resolution of Problem (3) to a subspace of the FE approximation space in which solutions are smooth. Section 2.2 investigates to which extent, FFD could be a good candidate for this purpose.

2.2. FFD-based acoustic solver

In this section, it is proposed to transpose the concept of FFD [9,26,27] to the approximation of the solution of a PDE (specifically, pressure field in this case). This method can be interpreted as a projection onto a reduced, smooth basis and has the interest to

be non-invasive with respect to existing efficient FE implementations of acoustic problems. For the presentation, the creation of the morphing box is first outlined; then, the link between the FE field and that of the morphing box is derived, and finally, the conditioning issues are properly managed before applying the strategy to the time-acoustic problem of interest. The basics of the FFD approach are intentionally presented concisely, with interested readers referred to previous contributions [9,26] for more details. Similarly, only the fundamentals of spline technology are recalled; for more information, see for example [5,10,11]. The emphasis is rather placed on presenting the method as a type of fictitious domain approach that is approximated and has the advantage of being non-invasive.

2.2.1. Creating the morphing box

The first step is to immerse the fine FE mesh into a bi- or tri-variate spline box. For simplicity and as most of the works dealing with FFD, B-spline functions are used for the morphing box. The B-spline box geometry is more precisely usually chosen as a one-patch B-spline with a dimension of d_{FFD}, which corresponds to either a rectangle for $d_{\text{FFD}} = 2$ or a rectangular parallelepiped for $d_{\text{FFD}} = 3$. For the sake of simplicity, the same polynomial order p is used for all parametric directions. Open uniform knot vectors $\Xi_j = \{\xi_j^1, \dots, \xi_j^{n_j+p+1}\}$ define the univariate B-spline basis functions $\tilde{N}_{i_k}^k$, for instance with $d_{\text{FFD}} = 3$:

$$\left(\tilde{N}_{i_1}^1\right)_{i_1\in 1,2,\dots,n_1}, \quad \left(\tilde{N}_{i_2}^2\right)_{i_2\in 1,2,\dots,n_2} \quad \text{and} \quad \left(\tilde{N}_{i_3}^3\right)_{i_3\in 1,2,\dots,n_3}. \tag{4}$$

n_1, n_2 and n_3 are the number of univariate basis functions in each parametric direction j, further details can be found in [9]. The multivariate B-spline basis function N_i at the ith control point (corresponding to control point $i_1, \dots, i_{d_{\text{FFD}}}$ in the different parametric directions) is obtained by the tensor product of the d_{FFD} univariate basis functions as follows:

$$N_i(\xi) = \tilde{N}_{i_1}^1(\xi_1) \times \tilde{N}_{i_2}^2(\xi_2) \times \tilde{N}_{i_3}^3(\xi_3), \tag{5}$$

where $\xi \in \mathbb{R}^{d_{\text{FFD}}}$. The B-spline surface, or volume B is then defined by:

$$B(\xi) = \sum_{i=1}^{n_{\text{FFD}}} N_i(\xi) X_i^{\text{FFD}} = \mathbf{N}^T(\xi)\mathbf{x}_{\text{FFD}}, \tag{6}$$

where $\mathbf{N}$ denote the matrix of the $n_{\text{FFD}} = n_1 \times \cdots \times n_{d_{\text{FFD}}}$ B-spline basis functions N_i and $\mathbf{x}_{\text{FFD}}$ the $d_{\text{FFD}} \times n_{\text{FFD}}$ vector gathering the coordinates $\{X_{1,i}^{\text{FFD}}, \dots, X_{d_{\text{FFD}},i}^{\text{FFD}}\}$ associated to control point i. The spline box topological dimension d_{FFD} depends on the dimension of the structure to be embedded, denoted by d. Indeed we necessarily have $d \le d_{\text{FFD}}$. The parametric domain and the control point positions are usually chosen so that the mapping from the parametric to the physical domain is identity. Thus, the coordinate $X_{j,i}^{\text{FFD}}$ of the control point i in the direction j (corresponding to control point i_j in this parametric direction), can be found by the Greville abscissae, given by :

$$\forall i_j \in [1, n_j], \quad X_{j,i}^{\text{FFD}} = \frac{1}{p} \sum_{k=i_j}^{i_j+p-1} \xi_j^k, \tag{7}$$

where ξ_j^k is the kth knot value of knot vector Ξ_j. In practice, this property is obtained directly by the spline refinement process, starting with one single element. The size of the spline box is determined such that the FE mesh is fully immersed in the Spline box. Next Section aims at bridging their functional spaces.

2.2.2. Link between DOFs of the FE mesh to that of the spline box

As the "D" in FFD stands for *Deformation*, the spirit of FFD was initially to control the deformations of the immersed geometry (here a FE mesh) by acting on the positions of the control points. This explains its use in shape optimization, as the unknown is the shape and the morphing box actually *deforms* its shape. It is proposed in this paper to extend the concept of *deformation* to any other field living in the immersed body. Namely, in the present context of acoustics, it is envisaged to link the FE pressure field (see (2)) to another smoother field discretized by the spline morphing box.

A first way to bridge the FE mesh to the spline box would be to evaluate the spline functions at any point x in the FE mesh. This would result in:

$$u^h(x) = \sum_{i=1}^{n_{\text{FFD}}} N_i(\mathcal{M}(x)) u_i^{\text{FFD}}, \tag{8}$$

where u_i^{FFD} would be equivalent pressure values at the spline box control points. Such a choice would be similar to the common practice in fictitious domain methods, where the conforming quadrature rule, usually built using octree meshes or subcells, would be replaced by an appropriate subdivision of the finite elements, the FE being already conforming. However, this approach appears too complex in this context, since it is highly invasive with respect to the FE code used to solve this kind of problems.

The goal here is rather to use the spline box to build a smooth reduced basis from the standard FE approximation. To do so, starting from the classic FE approximation (2), the key point is to apply the morphing box deformation *only* to the nodes of the FE mesh. Therefore, the FE DOF vector u_j^{FE} in (2) is now associated to a smaller B-spline DOF vector defined at the control points of the box through:

$$u_j^{\text{FE}} = \sum_{i=1}^{n_{\text{FFD}}} N_i\left(\xi_j^{\text{FE}}\right) u_i^{\text{FFD}}, \tag{9}$$

where ξ_j^{FE} corresponds to the position of the jth node in the parametric domain of the B-spline (i.e., here, to the actual position of the node in the physical space as a consequence of the identity mapping of the box). This leads to a conventional FE field, but where the FE DOFs are driven by the morphing box DOFs:

$$u^h(x) = \sum_{j=1}^{n_{\mathrm{FE}}} L_j(x) \sum_{i=1}^{n_{\mathrm{FFD}}} N_i\left(\xi_j^{\mathrm{FE}}\right) u_i^{\mathrm{FFD}}. \tag{10}$$

Remark. Given (10), let us note at this stage that the FFD technique produces new shape functions of form $\sum_{j=1}^{n_{\mathrm{FE}}} L_j(x) N_i\left(\xi_j^{\mathrm{FE}}\right)$, i.e., the FE approximation of the B-spline box shape functions. The proposed approach can therefore be regarded as a type of pointwise discretization of fictitious domain methods (see (8)). If the FE mesh was infinitely fine, it would be equivalent to the fictitious domain approach. However, since the proposed FFD method involves a FE field (see (10)), it is non-invasive with respect to standard FE codes. In other words, the proposed choice (10) can be seen as a non-invasive discrete approximation of the first one (8).

The FFD operator $\mathbf{R}_s$ is now introduced in matrix–vector notation so that (9) and (10) can be recast as:

$$u^h(X) = \mathbf{L}^T(X)\,\mathbf{u}_{\mathrm{FE}} \qquad \text{with} \qquad \mathbf{u}_{\mathrm{FE}} = \mathbf{R}_s^T \mathbf{u}_{\mathrm{FFD}}. \tag{11}$$

Operator $\mathbf{R}_s$ is a $(n_{\mathrm{FFD}} \times n_{\mathrm{FE}})$ matrix simply gathering the evaluation of each spline function at the nodes of the FE mesh, namely $\left(N_i\left(\xi_j^{\mathrm{FE}}\right)\right)_{(i,j)}$. This is straightforward to compute due to the choice of the identity mapping between the parametric and physical domains. From a practical point of view, operator $\mathbf{R}_s$ maps a FFD DOF vector $\mathbf{u}_{\mathrm{FFD}}$ to the FE one $\mathbf{u}_{\mathrm{FE}}$. As mentioned before, it can be interpreted as a smooth reduced basis as encountered in primitive model order reduction techniques [41–43]. Any FE linear system of form $\mathbf{A}_{FE}\,\mathbf{u}_{FE} = \mathbf{b}_{FE}$ is thus classically reduced with a Galerkin projection using $\mathbf{R}_s$, which leads to solving the following $n_{FFD} \times n_{FFD}$ system:

$$\underbrace{\mathbf{R}_s\,\mathbf{A}_{FE}\,\mathbf{R}_s^T}_{\mathbf{A}_{FFD}}\,\mathbf{u}_{FFD} = \underbrace{\mathbf{R}_s\,\mathbf{b}_{FE}}_{\mathbf{b}_{FFD}}. \tag{12}$$

The result is finally post-processed using (11). Once again, it consists in a conventional nodal FE field. This method has therefore the strong interest of being non-invasive with respect to a standard FE code, in the sense that classical quadrature rules and FE operator assembly can be applied and the connectivity of the elements remains the same. This means that the method can be easily implemented in existing conventional FE codes.

2.2.3. Conditioning issues: removing function and diagonal scaling

As with any immersed-like method [23–25], the support of the shape function of some control point may not intersect the embedded domain, which is here a FE mesh. This will result in a rank deficient FFD operator. Additionally, small intersection may result in an ill-conditioned operator. Both these problems must be considered and operator $\mathbf{R}_s$ should be corrected to improve its condition number. To achieve this, a first non-invasive strategy based on removing basis functions is used. It consists in removing columns in $\mathbf{R}_s$ that are zero or nearly zero according to a criterion following [9,26].

However, even in this situation, the condition number may be poor and require special treatment. For instance, simple preconditioning techniques were proposed to improve conditioning and restore standard mesh convergence [44–46]. Specifically, it is envisaged here to use a diagonal operator composed of the inverse of the norm of the columns of $\mathbf{R}_s$ to precondition the linear system, still in a non-invasive way. In practice, it is proposed to scale directly the FFD operator $\tilde{\mathbf{R}}_s = \mathbf{H}\mathbf{R}_s$ with the following diagonal operator $\mathbf{H}$:

$$\mathbf{H} = \begin{bmatrix} \frac{1}{\sqrt{(\mathbf{R}_s\mathbf{R}_s^T)_{11}}} & \cdots & 0 \\ \vdots & \ddots & \vdots \\ 0 & \cdots & \frac{1}{\sqrt{(\mathbf{R}_s\mathbf{R}_s^T)_{nn}}} \end{bmatrix}. \tag{13}$$

It is important to note that the construction of $\mathbf{H}$ is always possible according to the properties of the B-spline basis functions [11] and thanks to the above procedure for removing basis functions whose support weakly intersects the mesh. Indeed, this ensures that the product of $\mathbf{R}_s\mathbf{R}_s^T$ is always positive definite. Nonetheless, this additional scaling has no impact on the solution as the space remains unaltered. Such a diagonal preconditionner is not sufficient to *repair* quasi zero eigenvalues due to small intersections [24].

2.2.4. Back to the time-acoustics problem

Based on (11), the time-harmonic acoustic problem given in (3) can now be projected onto a spline box based basis by using the preconditioned FFD operator $\tilde{\mathbf{R}}_s$. Such a strategy is particularly relevant when applied to the acoustic simulation of musical instrument. As mentioned in section 2.1, performing the simulation of saxophone requires the resolution of hundreds of thousands of linear systems with an operator made of a linear combination of stiffness $\mathbf{K}_{\mathrm{FE}}$, mass $\mathbf{M}_{\mathrm{FE}}$ and Dirichlet $\mathbf{D}_{\mathrm{FE}}$ operators that are constant throughout the frequency bandwidth of interest. These operators can therefore be projected once for all the (tens of) thousands of frequencies of analysis. Only operator $\mathbf{\Sigma}_{\mathrm{FE}}$ corresponding to the non-linearity of the dissipation at the walls and to the radiation conditions have to be updated and thus projected (as $\tilde{\mathbf{R}}_s\mathbf{\Sigma}_{\mathrm{FE}}\tilde{\mathbf{R}}_s^T$) for each frequency value. But we recall that these terms are based on the boundaries, and therefore are highly sparse and relatively cheap to project. In the following, all the operators denoted by $\bullet_{\mathrm{FFD}}$ are projected onto the FFD subspace once for all frequency steps. Problem (3) thus becomes:

$$\left[\mathbf{K}_{\mathrm{FFD}} - \omega^2\mathbf{M}_{\mathrm{FFD}} + \tilde{\mathbf{R}}_s\mathbf{\Sigma}_{\mathrm{FE}}\tilde{\mathbf{R}}_s^T + \mathbf{D}_{\mathrm{FFD}}\right]\mathbf{u}_{\mathrm{FFD}} = \mathbf{b}_{\mathrm{FFD}}, \tag{14}$$

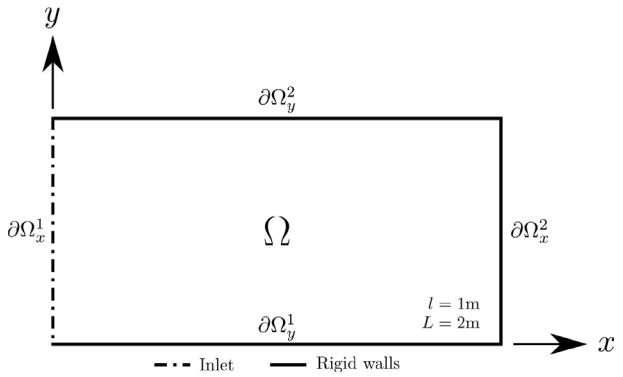

Fig. 1. 2D problem setting: a rectangle domain submitted to prescribed pressure (Dirichlet) on the left hand side $\partial\Omega_x^1$ and rigid walls (Neumann) on the 3 other boundaries $\partial\Omega_x^2, \partial\Omega_y^1$ and $\partial\Omega_y^2$.

with the constant projected operators:

$$\mathbf{K}_{\text{FFD}} = \tilde{\mathbf{R}}_s\, \mathbf{K}_{\text{FE}}\, \tilde{\mathbf{R}}_s^T, \qquad \mathbf{M}_{\text{FFD}} = \tilde{\mathbf{R}}_s\, \mathbf{M}_{\text{FE}}\, \tilde{\mathbf{R}}_s^T, \tag{15}$$

$$\mathbf{D}_{\text{FFD}} = \mu\, \tilde{\mathbf{R}}_s\, \mathbf{D}_{\text{FE}}\, \tilde{\mathbf{R}}_s^T \quad \text{and} \quad \mathbf{b}_{\text{FFD}} = \mu\, \tilde{\mathbf{R}}_s\, \mathbf{D}_{\text{FE}}\, \mathbf{u}_{\text{FE}}^d. \tag{16}$$

Last, to post-process the computed FFD pressure field $\mathbf{u}_{\text{FFD}}$ it is usually more convenient to compute the corresponding FE DOF vector $\mathbf{u}_{\text{FE}}$ using (11) and rely on existing FE post-processing procedures.

3. Numerical results

In this section, the performance of the FFD method is evaluated on a series of problems of increasing difficulty. In Section 3.1, several simple two-dimensional cases with a closed-form solution are analyzed to study the performance and convergence of the method, both in conforming and non-conforming configurations. In Section 3.2, the method is applied to a realistic musical acoustics problems. It gives an idea of the gains that can be achieved using this approach on complex industrial use-cases.

3.1. 2D academic examples

An academic two-dimensional acoustic problem with closed-form solution is presented in Section 3.1.1. The convergence of the FFD method is studied in a first configuration, referred to as *conforming*, where the domain covered by the spline box is strictly equal to Domain Ω , in Section 3.1.2 Then, a *non-conforming* configuration where Ω is an arbitrary subdomain of the spline box, is studied in Section 3.1.3.

3.1.1. Problem setting

The test case analyzed here is inspired from the acoustic isogeometric analysis performed in [12]. Let us consider a rectangular domain of $L = 2$m width and $l = 1$m height, denoted Ω, see Fig. 1.

The lower, upper, and right walls are assumed rigid (i.e. homogeneous Neumann condition $v \cdot n = 0$). The inlet (left wall) is subjected to a non-homogeneous Dirichlet boundary condition. The Helmholtz problem in Ω is: find $u(x, y)$ such that

$$\begin{cases} \Delta u + k^2 u = 0, & \text{in } \Omega, \\ u(0, y) = \bar{u}_0 \cos\left(\frac{m_y \pi}{l} y\right), & \text{on } \partial\Omega_x^1, \\ v(x, y) \cdot n = 0, & \text{on } \partial\Omega_y^1,\ \partial\Omega_y^2,\ \text{and } \partial\Omega_x^2, \end{cases} \tag{17}$$

where $m_y \in \mathbb{N}$ and $\bar{u}_0 = 1$ Pa are the mode number in the y-direction and the magnitude of the prescribed pressure on $\partial\Omega_x^1$ respectively. Problem (17) is solved for different wave-numbers $k \in \mathbb{R}^+$.

As stated above, there is a closed-form solution to this problem, which reads:

$$u^{\text{ref}}(x, y) = \cos\left(\frac{m_y \pi}{l} y\right) \left(A_1 e^{-jk_x x} + A_2 e^{jk_x x}\right), \tag{18}$$

with A_1 and A_2 solutions of the following linear system:

$$\begin{bmatrix} 1 & 1 \\ e^{-ik_x L} & e^{ik_x L} \end{bmatrix} \begin{bmatrix} A_1 \\ A_2 \end{bmatrix} = \begin{bmatrix} u_0 \\ 0 \end{bmatrix}, \tag{19}$$

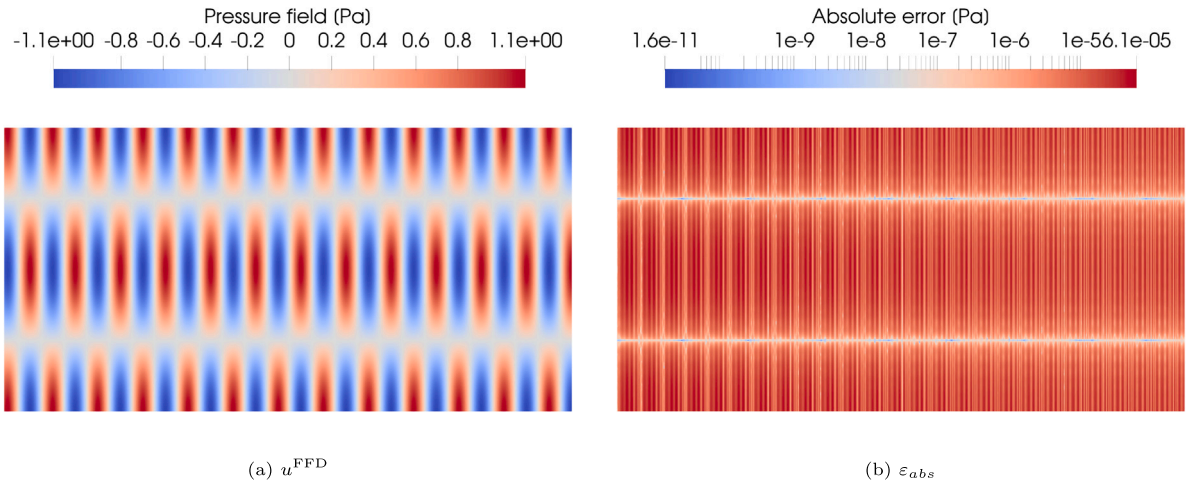

(a) u^{FFD} (b) ε_{abs}

Fig. 2. 2(a) Numerical solution of pressure field obtained by using the FFD method for $m = 3$, $n_\lambda^{\mathrm{FFD}} = 20$ and 2(b) the corresponding relative error map ε_{abs} with a logarithmic scale colormap.

and with $k_x = \sqrt{k^2 - \left(\frac{m_y \pi}{l}\right)^2}$. A reference FE DOF vector $\mathbf{u}_{\mathrm{ref}}$ was constructed from the evaluation of the closed-form solution $u^{\mathrm{ref}}(x, y)$ at the nodes of the FE mesh. To assess the quality of a FFD solution $\mathbf{u}_{\mathrm{FFD}}$, its equivalent DOF vector $\mathbf{u}_{\mathrm{FE}}^{\mathrm{FFD}} = \mathbf{R}_s^T \mathbf{u}_{\mathrm{FFD}}$ was computed. The quality is then quantified using the relative L^2-norm ε_{L_2} defined by:

$$\varepsilon_{L_2} = \frac{\|\mathbf{u}_{\mathrm{ref}} - \mathbf{u}_{\mathrm{FE}}^{\mathrm{FFD}}\|^2}{\|\mathbf{u}_{\mathrm{ref}}\|^2} \tag{20}$$

In this paper, all the FE operators were obtained using the open-source computational environment DOLFINx [47] of FEniCS Project. The linear systems were solved using MUMPS parallel sparse direct solver [48].

3.1.2. Conforming case

In this section, the conforming configuration is considered first. The problem (17) has been solved in Ω with mode number $m_y = 2$ and wavenumber $k = 40$. Ω was meshed with 9-node quadratic quadrilaterals finite elements while the morphing box was meshed with cubic ($p = 3$) splines. In the following, the discretization densities of both meshes are parametrized by the number of elements per wavelength $n_\lambda = h/\lambda$ where $\lambda = 2\pi/k$ the wavelength. In the following, the FE mesh density was set to $n_\lambda^{\mathrm{FE}} = 40$, corresponding to 164.059 DOFs and the spline box was set to $n_\lambda^{\mathrm{FFD}} = 20$ corresponding to 11.094 DOFs. For all simulations, the penalization parameter was set to $\mu = 10^5 \rho_A$ where ρ_A is the spectral radius of the operator $\mathbf{A}_{\mathrm{FE}}$.

The FFD system (14) was solved for this problem. The computed pressure field u^{FFD} is shown in Fig. 2(a) and the corresponding relative error map with respect to the closed-form solution $\varepsilon_{abs} = |\mathbf{u}_{\mathrm{ref}} - \mathbf{u}_{\mathrm{FE}}^{\mathrm{FFD}}|/u_0$ is given in Fig. 2(b). With such a parametrization, the FFD method demonstrates its ability to produce a result that is close to the theoretical pressure field since the maximum local relative error is less than 10^{-5}.

To further investigate the behavior of the method, a convergence study similar to [12] is presented in Fig. 3 with $m_y = 2$ and $k = 10$. The idea was to compare the results of the proposed non-invasive FFD-based implementation with the full isogeometric acoustic analysis of [12]. A fixed FE mesh with $n_\lambda^{\mathrm{FE}} = 400$ was chosen and the pressure $\mathbf{u}_{\mathrm{FFD}}$ was then calculated using a spline box with a mesh density of n_λ^{FFD} ranging from 4 to 21 for $p = \{2, 3, \ldots, 6\}$.

Fig. 3 shows the L^2 error (20) of the FFD solution as a function of the spline mesh density for the different spline degrees. The same convergence results as in [12] were obtained, validating the implementation and the ability of the method to compute the spline solution in a non-invasive way from a finite element library.

A second convergence analysis was then carried out more in the spirit of projection-based model order reduction. Indeed, we recall that our primary objective was to find a smooth regular subspace within the C^0 FE approximation space that is capable of providing the same level of accuracy with a smaller number of degrees of freedom. To demonstrate the potential of the method, for different spline degrees p and for different FE mesh refinements $n_\lambda^{\mathrm{FE}} \in \{40, 72, 104, 136, 168, 200\}$, the minimum ratio $r = n_\lambda^{\mathrm{FFD}}/n_\lambda^{\mathrm{FE}}$ was iteratively sought such that the FFD solution maintained the same level of accuracy in L_2-norm as the classical FE solution. Fig. 4 presents the corresponding results. First, the black dashed line reflects the classical FE convergence, namely, the relative L_2-error as a function of the number of DOFs for 6 different meshes. For each mesh, the FFD was applied with a spline box of degree $p = \{2, 3, 4, 5, 6\}$. For $p = 2$ the ratio r was limited to 1 (i.e. B-spline elements have the same size as FE elements).

It can be seen that all the FFD curves are significantly shifted to the left. This means that, for this simple problem, it is possible to find a regular subspace of much smaller size that provides the same level of accuracy as the FE approximation subspace with minimal invasiveness with respect to the FE package. For this simple example, the ratio r actually decreases sharply from 1 to 0.16

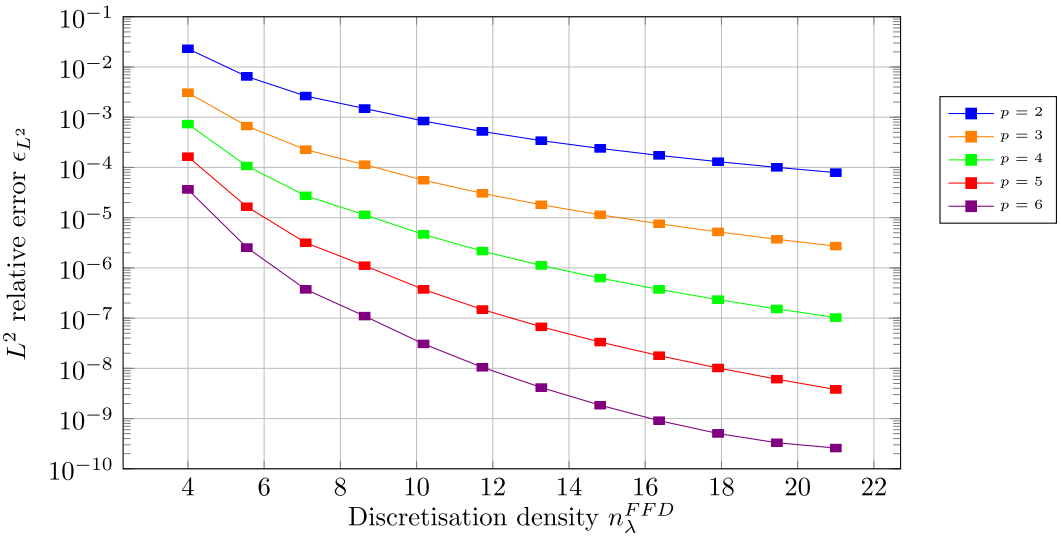

Fig. 3. Evolution of the L_2 relative error ε_{L_2} versus the discretization density n_λ^{FFD} for $k = 10$ and $p = 2, \ldots, 6$.

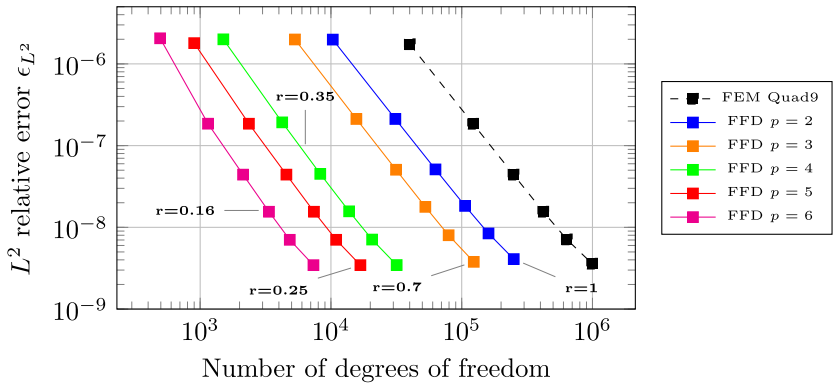

Fig. 4. Illustration of the potential of the proposed FFD method with optimal ratio $r = n_\lambda^{\text{FFD}}/n_\lambda^{\text{FE}}$ to reduce the number of DOFs while keeping the same level of relative L_2 error for different FE meshes and spline box degrees $p = \{2, 3, \ldots, 6\}$.

with p, as shown in the Fig. 4 . It must be stressed that, for this very simple example (smooth solution and smooth geometry), with spline degrees 2 or 3, it is possible to reduce the number of DOFs by 3 to almost 10 for the same level of accuracy, and by more than two orders of magnitude with degree 6.

3.1.3. Non-conforming case

The robustness of the FFD method is now examined by solving a non-conforming 2D problem. Recall that *non-conforming* means that the analysis domain Ω is a subdomain of the spline box and that it may partially and arbitrarily intersect spline elements. For this, the problem of Section 3.1.1 is considered again with the fine mesh of Fig. 3 and a spline box with an element of 40 mm, but this time, the domain Ω is rotated within the spline box with arbitrary angles ranging between $\alpha = 0$ and $\alpha = \pi/2$, as shown in Fig. 5.

The advantage is that the closed-form solution (18) still holds in the rotated coordinate system, allowing for error quantification. The spline box, a square structure with a homogeneous element size in all directions, was used to ensure equal number of control points for $\alpha = 0$ and $\pi/2$. The size of the spline box was chosen to be much larger than the domain Ω in order to minimize the influence of control points collected around the edges of the spline box. This study was carried out for $m_y = 0$ and 2 and with a wave number equal to $k = 10$.

The results of this study are presented in Fig. 6 with (solid line) and without (dashed line). The first observation is that, in the absence of the preconditioner of Section 2.2.3, the FFD method does not show a stable behavior of the error in the nonconforming case, especially for high spline degrees. Conversely, the proposed scaling method restores the good spectral properties of the operator and allows the method to behave very robustly, even for high order spline boxes. In view of this first result, it appears that preconditioning is essential for the method to work efficiently.

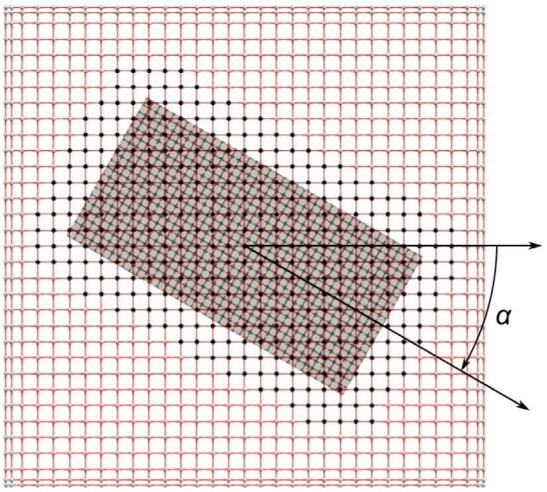

Fig. 5. Parametrization of the robustness study. An example of a spline box (control mesh in red) with $p = 3$ in the configuration where $\alpha = \pi/6$. The control DOFs in black were kept while the white ones were removed according to the selection strategy of Section 2.2.3.

Secondly, it can be noticed that the solution computed with the preconditioned FFD method is almost invariant with the angle of rotation, whereas very arbitrary configurations of the intersection of the domain with the spline box are considered by its variation between 0 and π. Thirdly, a significant decrease in ε_{L_2} is also observed with spline degree p, as expected from the conclusion of the conforming case study.

More precisely, it can be observed that the L_2 error analysis reaches a (local) minimum around $\pi/4$ for both $m_y = 0$ and $m_y = 2$ configurations. In fact, the error decreases slightly at $\pi/4$. This can be explained by the fact that the number of control points (and therefore the number of DOFs) in the domain Ω evolves with the rotation. In fact, the number of active control points reaches its maximum at $\alpha = \pi/4$. Therefore the approximation space thus increases a bit, which slightly improves the approximation.

For $m_y = 2$ the result remains largely unchanged. A general increase in the order of magnitude of the L_2 relative error can be observed due to the increase in the solution complexity. It can also be seen that the error for $\alpha = 0$ and $\alpha = \pi/2$ has very low error values. This is due to the fact that the closed-form solution of the problem has a first-order tensor representation (product of a function of x and a function of y) which is well captured when the domain is aligned with the axis of the spline box.

In conclusion, the proposed preconditioned FFD approach is robust to arbitrary intersections of the domain with the spline box making it a good candidate for reducing problems in complex shape domains such as musical instruments.

3.2. Application to a real saxophone body

The proposed method is now applied to a 3D industrial application case with a complex geometry, corresponding to the analysis of an alto saxophone body (model Henri Selmer Paris - SERIES III) with 19 tone holes, as shown in Fig. 7. The acoustic quality of such musical instruments is generally quantified by the input impedance of the resonator [49]. More specifically, the input impedance Z_{in} is defined by the Eq. (21).

$$Z_{in} = \frac{p_{in}}{v_{in}^{\perp}} = \frac{\int_{S_p} \hat{p} d\Gamma}{\int_{S_p} \hat{v} \cdot -n d\Gamma} = j\rho\omega \frac{\int_{S_p} \hat{p} d\Gamma}{\int_{S_p} \nabla \hat{p} \cdot n d\Gamma}. \tag{21}$$

From the analysis of its resonance frequencies, we can estimate its tuning, homogeneity, harmony, playability or timbre. It is therefore of vital interest to instrument makers. The error on the normalized input impedance $Z = \frac{Z_{in}}{\rho c}$ is studied in terms of the cent deviation on the resonant frequencies. A cent is a logarithmic unit used to quantify the musical interval between two notes of frequencies f_1 and f_2:

$$\varepsilon_{cent}(f_1, f_2) = 1200 \log_2 \left(\frac{f_2}{f_1} \right) \tag{22}$$

A cent is defined as a hundredth of a tempered semitone. It is assumed that the difference between two notes is imperceptible below 14 cents. To design world-class instruments, manufacturers require less than 10 cents of error. For example, a model is considered accurate enough if the difference between the predicted f_{sim} and the measured f_{exp} frequency of the resonances is such that $\varepsilon_{cent}(f_{sim}, f_{exp}) < 10$ c. In this context, for the purposes of this research, the errors between frequencies are quantified in cents.

To well predict the impedance and to accurately define the chimneys and other intricate geometries, a quadratic mesh of ≈785,000 quadratic 10 nodes tetrahedrons was required [3]. The maximum cell size was set to 2 mm, which is well below $\lambda/10$ at

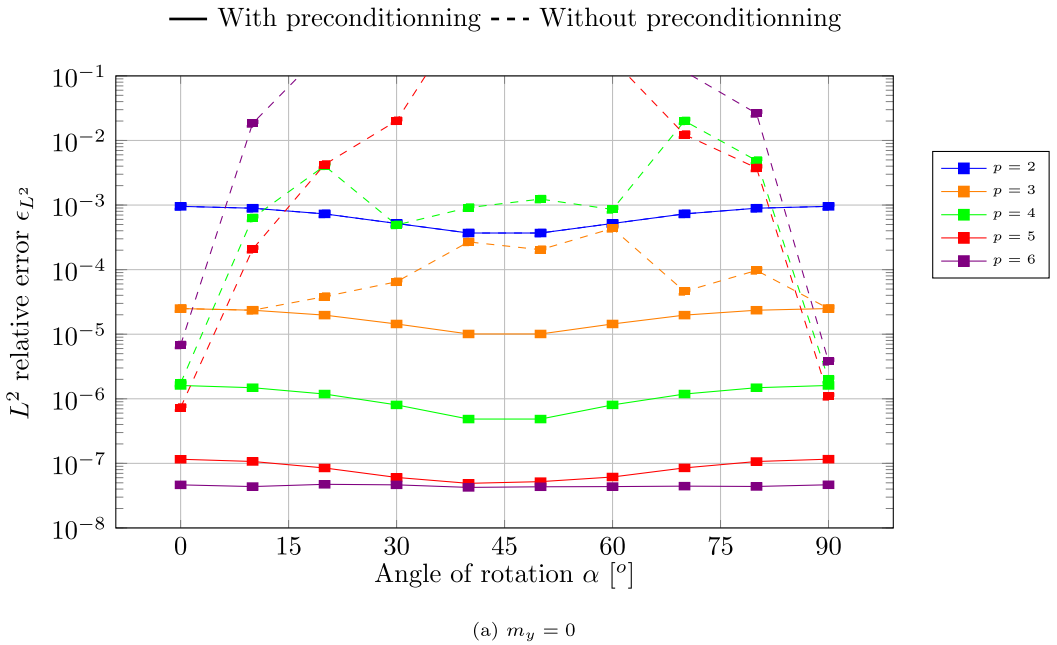

(a) $m_y = 0$

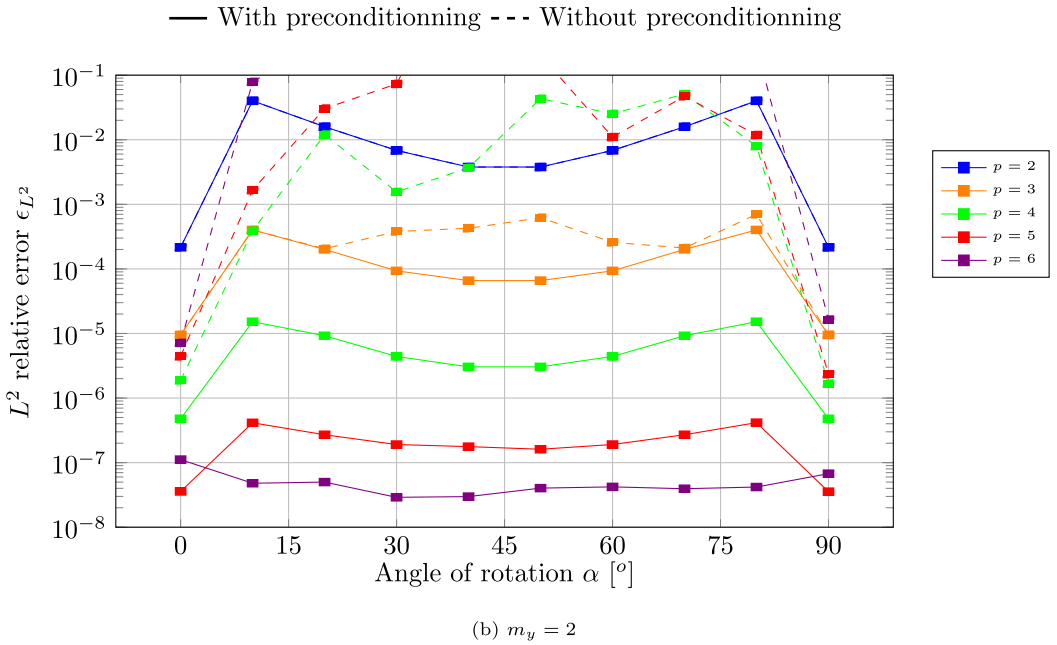

(b) $m_y = 2$

Fig. 6. Evolution of the L_2 relative error versus the rotation angle α of the domain Ω. 6(a) mode number $m_y = 0$ (i.e. no wave on y) and 6(b) $m_y = 2$.

8 kHz. The face size at the walls was set to 1 mm and the mesh was also refined in the tone hole regions as shown in the zoom of Fig. 7. Radiation in the external domain was accounted for by a static condensation technique, so that only the internal air volume of the instrument was discretized according to [3]. In a nutshell, spheres centered on each open chimney are added to the study domain to simulate (i) radiation conditions at infinity and (ii) the outer face of the body and the presence of keys. To reduce the complexity of the calculations and thanks to some modeling assumptions, it is possible to condense the operators of each sphere, in the spirit of Guyan's static condensation. The study domain is thus reduced to the bore only with non-standard impedance conditions on each open chimney. The resulting acoustic problem on the bore of the instrument consisted of approximately 1.2 million DOFs. The study considered three fingerings out of the 50 possible ones. As shown in the left part of Fig. 8, they differ in the combination of open tone holes (shown in green in the figure) or, in other words, with different boundary conditions at the holes. More specifically, the fingerings considered correspond to D#4, F4 and A#4p respectively.

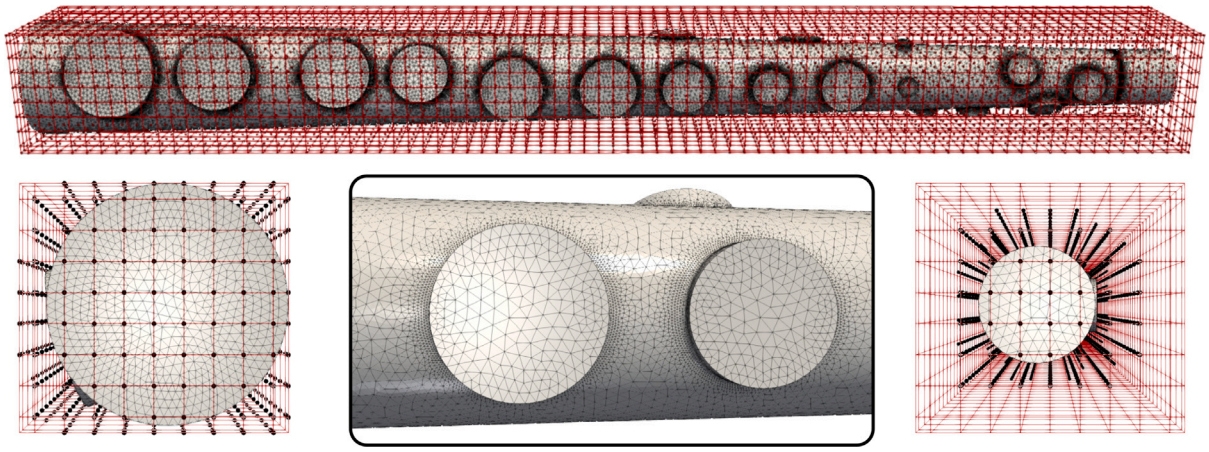

Fig. 7. Tet10 FE mesh of the saxophone body with the corresponding quadratic $p = 2$ spline box, represented by its control mesh (in red). The black dots represent the control points actually used in the FFD projection. (For interpretation of the references to color in this figure legend, the reader is referred to the web version of this article.)

A parallelepiped spline box was chosen with homogeneous element size in all directions, every 6 mm, and a spline polynomial degree $p = 2$ was chosen for all parametric directions, so that the initial number of control points (and thus degrees of freedom) in the morphing box consisted of only 9020 unknowns. The control mesh is shown in red in Fig. 7. Following the correction procedure of Section 2.2.3, 2778 (about 30%) control points were removed because they did not (sufficiently) intersect the FE mesh. The total number of active degrees of freedom of the FFD morphing box drops to only 6242, shown as black dots in Fig. 7. This is a drastic reduction in terms of DOFS as it corresponds to 0.8% of the size of the FE problem.

All calculations were performed on an (Intel(R) Xeon(R) Gold 6230 CPU @ 2.10 GHz machine, with 2 sockets of 20 CPU - 40 threads each, and 126 Go total RAM. The resulting pressure field was calculated following the approach described in previous work [3] for the reference FE approach and the presented FFD method.

The impedance for the three fingerings is shown in figure Fig. 8. For the three fingerings, a very good agreement is obtained between the full FE simulation (blue) and the proposed FFD reduction technique (red). Not only the resonance frequencies, but also the phase and magnitude of the peaks are reproduced exceptionally well with much fewer degrees of freedom. To go further, the histogram of Fig. 9 shows the deviations between the FE and FFD approaches for the three fingerings considered.

FFD gives satisfactory approximations to FEM at much lower cost, with deviations of less than 10 cents for the six resonances studied. Only A#4p shows differences greater than 10 cents for the second peak, but it is still considered imperceptible since it is below 14 cents. This can be explained by the fact that this fingering is much more complex, since it corresponds to many open holes, which are very close to each other, with possible external interactions.

Remark. It is worth mentioning that the morphing box and the mesh cannot be determined completely independently or arbitrarily. Indeed, there must be sufficient finite element nodes in each spline element to ensure the orthogonality of the spline modes. In particular, a spline element must not be smaller than a finite element. Logically, this type of situation should not occur if FFD is being used to reduce the model (or the number of DOFs). However, when the size of the finite elements is highly heterogeneous (very small and very large elements in the same mesh), then this situation can occur. There are two main ways of getting round this problem: (i) artificially refining the FE mesh in areas where it is really too coarse, or (ii) coarsening the morphing box locally, using hierarchical B-splines, for example.

Next, a comparison to experiments was performed in Fig. 10. It illustrates the deviations of the 6 resonances between both FEM $\varepsilon_{cent}(f_{FEM}, f_{exp})$ and FFD $\varepsilon_{cent}(f_{FFD}, f_{exp})$ from experimental measurements. Apart from some resonances of the complex A#4p fingering, all results are below the 10 cent criterion. The large deviations for the last fingering are mainly due to modeling assumptions or experimental biases, rather than the approximation of FFD vs. FEM, since pure FEM does not meet precision requirements either. Further explanations of these limits can be found in [3].

By reducing the number of DOFs by more than two decades, the computational burden is greatly reduced. This is especially true in the context of multiresolution, where most operators depend linearly or affinely on k. Specifically, the resolution of the linear system associated with the acoustic problem for one fingering at one frequency step using the standard finite element method takes 50 s on 8 processors and is reduced to 0.6 s on one single processor using the proposed FFD projection method. Taking into account the pre-processing (including the construction of the spline box from the FE mesh and assembly of $\mathbf{D}_{\text{FFD}}$) and projection steps, the computational cost is reduced by more than an order of magnitude.

4. Conclusion

In this paper, a non-invasive free-form deformation method based on B-splines has been extended to solve efficiently partial differential equations in complex domains. More precisely, the problem consists here in solving the scalar Helmholtz equation in

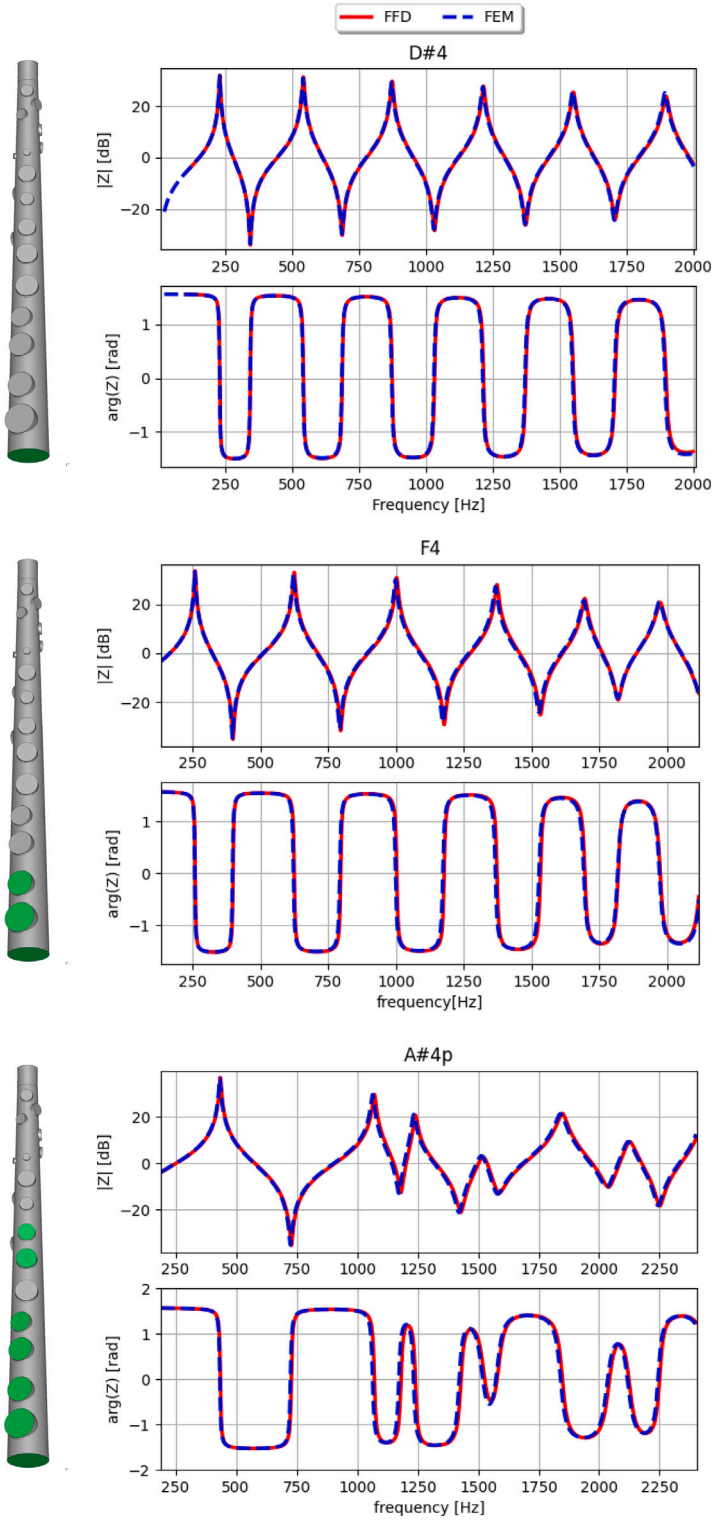

Fig. 8. Comparison of the impedance predicted by the proposed FFD modeling strategy (solid red) and FEM (dashed blue) for the 3 configurations: D#4 (top), F4 (middle) and A#4p (bottom). On the left side, the corresponding fingerings (open toneholes in green) and on the right the magnitude (top) and phase (bottom). (For interpretation of the references to color in this figure legend, the reader is referred to the web version of this article.)

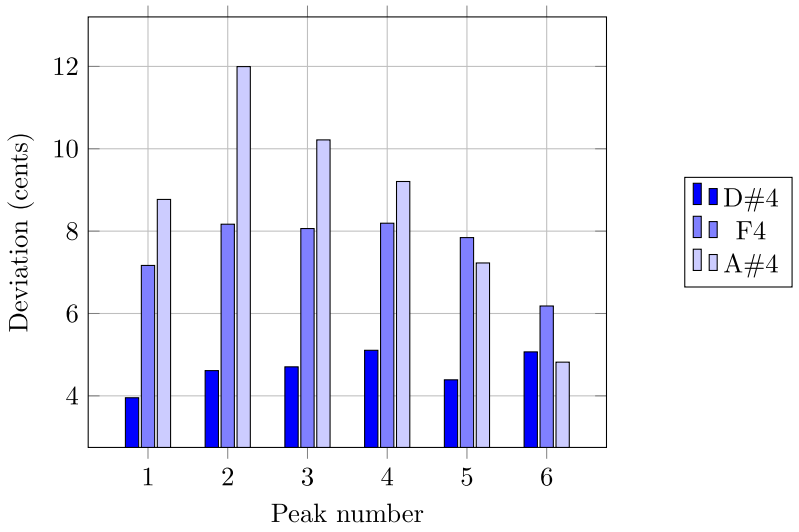

Fig. 9. Deviations in cents between the FFD and FEM modeling.

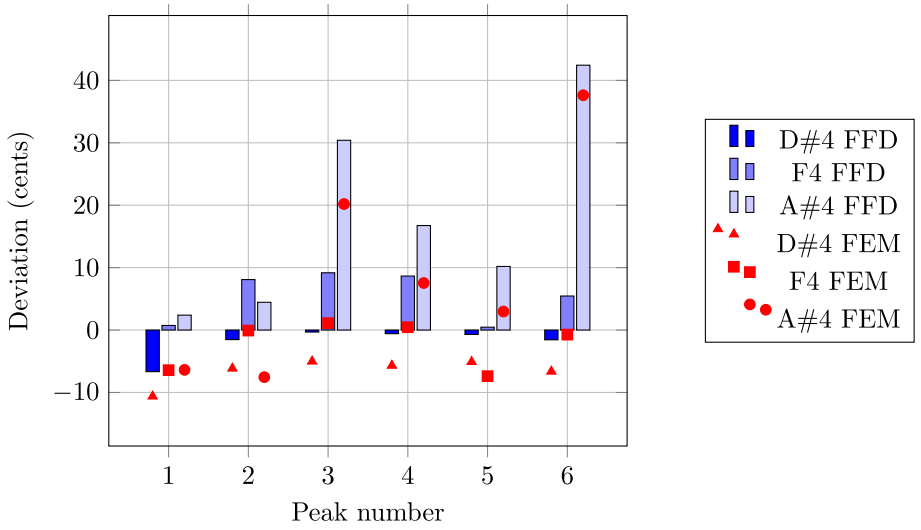

Fig. 10. Deviations in cents between the FFD and EXP modeling.

complex shaped musical instruments. To accurately represent the latter, the very fine finite elements used typically lead to large linear systems of equations, regardless of the complexity of the pressure field.

By restricting the analysis to a regular subspace of the FE approximation space, the proposed method allows to drastically reduce the computational cost. Not only is the number of unknowns reduced, but a high degree of sparsity of the resulting operator is maintained, which is usually not the case with classic projection-based model order reduction. Additionally, the proposed method is non-invasive and thus very easy to implement even in commercial FE tools (provided that (i) it can export the stiffness matrix and the right-hand side vector and (ii) it can get back a DOF vector computed externally). Lastly, the method is particularly well-suited to multiresolution parametric problems like time resolved PDE with linearly or affinely parametrized operators since projection is done once for all. Thanks to specific conditioning treatment, it was shown that the method is also very robust to arbitrary intersection of the spline box with the FE mesh.

In the last real-like example, the number of degrees of freedom was reduced by more than two orders of magnitude compared to the standard practice in finite element simulation of musical instruments. The number of DOFs was reduced from 1,200,000 to 6242, while both simulations produced comparable results in terms of accuracy. The total computation time was reduced by more than an order of magnitude which is a huge improvement for an instrument maker.

The developed method could be straightforwardly applied to many other problems posed over complex domains. Among the perspectives, extending the concept to non-parallelepipedic spline boxes would be interesting to better adapt the spline

approximation to the FE mesh. Adaptive strategies [50,51] could also be developed to adjust the spline box discretization to the FE mesh. In this context, it must be mentioned that it is much more convenient to adapt the spline box parameters with a fixed FE mesh, since the projection of the FE operators would be performed only once per spline box. Our method could also be a good candidate to relax some meshing constraints in complex domains [33].

CRediT authorship contribution statement

Marie Jeanneteau: Writing – original draft, Investigation, Data curation, Conceptualization. **Théo Sentagne:** Writing – original draft, Investigation. **Paul Oumaziz:** Writing – original draft, Supervision, Investigation, Conceptualization. **Robin Bouclier:** Writing – review & editing, Investigation, Conceptualization. **Jean-Charles Passieux:** Writing – original draft, Supervision, Investigation, Conceptualization.

Declaration of competing interest

The authors declare that they have no known competing financial interests or personal relationships that could have appeared to influence the work reported in this paper.

Data availability

The authors do not have permission to share data.

Acknowledgments

This work was supported by the ANRT, France through grant CIFRE-2019-1971 in collaboration with Henri Selmer Paris (HSP). Both ANRT and HSP are gratefully acknowledged. For the purpose of Open Access, a [CC-BYpubliccopyrightlicense] has been applied by the authors to the present document and will be applied to all subsequent versions up to the Author Accepted Manuscript arising from this submission.

References

[1] T.J. Hughes, The Finite Element Method: Linear Static and Dynamic Finite Element Analysis, Courier Corporation, 2012.
[2] O. Zienkiewicz, R. Taylor, J. Zhu, The Finite Element Method: Its Basis and Fundamentals, seventh ed., Butterworth-Heinemann, Oxford, 2013.
[3] M. Jeanneteau, P. Oumaziz, J. Passieux, V. Gibiat, J. Cottier, A combinatorial model reduction method for the finite element analysis of wind instruments, Int. J. Numer. Methods Eng. Prod. (2024) http://dx.doi.org/10.1002/nme.7582.
[4] T.J. Hughes, J.A. Cottrell, Y. Bazilevs, Isogeometric analysis: CAD, Finite Elements, NURBS, exact geometry and mesh refinement, Comput. Methods Appl. Mech. Engrg. 194 (39–41) (2005) 4135–4195.
[5] J.A. Cottrell, T.J. Hughes, Y. Bazilevs, Isogeometric Analysis: Toward Integration of CAD and FEA, John Wiley & Sons, 2009.
[6] T.J. Hughes, A. Reali, G. Sangalli, Duality and unified analysis of discrete approximations in structural dynamics and wave propagation: comparison of p-method finite elements with k-method NURBS, Comput. Methods Appl. Mech. Engrg. 197 (49–50) (2008) 4104–4124.
[7] J.A. Evans, Y. Bazilevs, I. Babuška, T.J. Hughes, n-widths, sup–infs, and optimality ratios for the k-version of the isogeometric finite element method, Comput. Methods Appl. Mech. Engrg. 198 (21–26) (2009) 1726–1741.
[8] S. Morganti, F. Auricchio, D. Benson, F. Gambarin, S. Hartmann, T. Hughes, A. Reali, Patient-specific isogeometric structural analysis of aortic valve closure, Comput. Methods Appl. Mech. Engrg. 284 (2015) 508–520.
[9] R. Bouclier, J.-C. Passieux, IGA: Non-Invasive Coupling with FEM and Regularization of Digital Image Correlation Problems, (no. 1) Wiley, 2023.
[10] E. Cohen, T. Lyche, R. Riesenfeld, Discrete b-splines and subdivision techniques in computer-aided geometric design and computer graphics, Comput. Graph. Image Process. 14 (2) (1980) 87–111.
[11] L. Piegl, W. Tiller, The NURBS Book, Springer Science & Business Media, 2012.
[12] T. Khajah, X. Antoine, S.P.A. Bordas, B-Spline FEM for time-harmonic acoustic scattering and propagation, J. Theor. Comput. Acoust. 27 (03) (2019) 1850059.
[13] V.K. Ummidivarapu, H.K. Voruganti, T. Khajah, S.P.A. Bordas, Isogeometric shape optimization of an acoustic horn using the teaching-learning-based optimization (tlbo) algorithm, Comput. Aided Geom. Design 80 (2020) 101881.
[14] H. D.J. Barucq, H.F.S. Calandra, Polynomial-reproducing spline spaces from fine zonotopal tilings, J. Comput. Appl. Math. 402 (2022).
[15] M.J. Borden, M.A. Scott, J.A. Evans, T.J. Hughes, Isogeometric finite element data structures based on Bézier extraction of NURBS, Internat. J. Numer. Methods Engrg. 87 (1–5) (2011) 15–47.
[16] D. Schillinger, P.K. Ruthala, L.H. Nguyen, Lagrange extraction and projection for NURBS basis functions: A direct link between isogeometric and standard nodal finite element formulations, Internat. J. Numer. Methods Engrg. 108 (6) (2016) 515–534.
[17] M. Tirvaudey, R. Bouclier, J.-C. Passieux, L. Chamoin, Non-invasive implementation of nonlinear isogeometric analysis in an industrial FE software, Eng. Comput. 37 (1) (2020) 237–261.
[18] G. Colantonio, M. Chapelier, R. Bouclier, J.-C. Passieux, E. Marenić, Non-invasive multilevel geometric regularization of mesh-based 3D shape measurement, Int. J. Numer. Methods Eng. 121 (9) (2020) 1877–1897.
[19] J. Videla, C. Anitescu, T. Khajah, S.P. Bordas, E. Atroshchenko, H- and p-adaptivity driven by recovery and residual-based error estimators for pht-splines applied to time-harmonic acoustics, Comput. Math. Appl. 77 (9) (2019) 2369–2395.
[20] L. Kudela, N. Zander, T. Bog, S. Kollmannsberger, E. Rank, Efficient and accurate numerical quadrature for immersed boundary methods, Adv. Model. Simul. Eng. Sci. 2 (2015) 1–22.
[21] X. Wei, B. Marussig, P. Antolin, A. Buffa, Immersed boundary-conformal isogeometric method for linear elliptic problems, Comput. Mech. 68 (6) (2021) 1385–1405.
[22] W. Garhuom, A. Düster, Non-negative moment fitting quadrature for cut finite elements and cells undergoing large deformations, Comput. Mech. 70 (5) (2022) 1059–1081.

[23] D. Schillinger, M. Ruess, The finite cell method: A review in the context of higher-order structural analysis of cad and image-based geometric models, Arch. Comput. Methods Eng. 22 (2015) 391–455.
[24] F. de Prenter, C.V. Verhoosel, E.H. van Brummelen, J.A. Evans, C. Messe, J. Benzaken, K. Maute, Multigrid solvers for immersed finite element methods and immersed isogeometric analysis, Comput. Mech. 65 (3) (2020) 807–838.
[25] A. Rouwane, R. Bouclier, J.-C. Passieux, J.-N. Périé, Adjusting fictitious domain parameters for fairly priced image-based modeling: Application to the regularization of digital image correlation, Comput. Methods Appl. Mech. Engrg. 373 (2021) 113507.
[26] M. Chapelier, R. Bouclier, J.-C. Passieux, Free-form deformation digital image correlation (FFD-DIC): A non-invasive spline regularization for arbitrary finite element measurements, Comput. Methods Appl. Mech. Engrg. 384 (2021) 113992.
[27] T. Sederberg, S. Parry, Free-form deformation of solid geometric models, 20, 1986, pp. 151–160.
[28] T. Lassila, G. Rozza, Parametric free-form shape design with PDE models and reduced basis method, Comput. Methods Appl. Mech. Engrg. 199 (23–24) (2010) 1583–1592.
[29] D.A. Burdette, J.R. Martins, Design of a transonic wing with an adaptive morphing trailing edge via aerostructural optimization, Aerosp. Sci. Technol. 81 (2018) 192–203.
[30] M. Chapelier, R. Bouclier, J.-C. Passieux, Spline-based specimen shape optimization for robust material model calibration, Adv. Model. Simul. Eng. Sci. 9 (1) (2022) 4.
[31] H. Zhao, D. Kamensky, J.-S. Hwang, John T. Chen, Automated shape and thickness optimization for non-matching isogeometric shells using free-form deformation, Eng. Comput. (2024) 1435–5663.
[32] D. Rueckert, P. Aljabar, Non-rigid registration using free-form deformations, in: Handbook of Biomedical Imaging, Springer, 2015, pp. 277–294.
[33] J.E. Fromm, N. Wunsch, R. Xiang, H. Zhao, K. Maute, J.A. Evans, D. Kamensky, Interpolation-based immersed finite element and isogeometric analysis, Comput. Methods Appl. Mech. Engrg. 405 (2023) 115890.
[34] H. Tijdeman, On the propagation of sound waves in cylindrical tubes, J. Sound Vib. 39 (1) (1975) 1–33.
[35] L. Cremer, On the acoustic boundary layer outside a rigid wall, Arch. Elektr. Uebertr 235 (2) (1948).
[36] A. Lefebvre, Computational Acoustic Methods for the Design of Woodwind Instruments (Ph.D. thesis), McGill University, Montreal, Canada, 2010.
[37] L. Chen, H. Lian, H.-W. Dong, P. Yu, S. Jiang, S.P. Bordas, Broadband topology optimization of three-dimensional structural-acoustic interaction with reduced order isogeometric fem/bem, J. Comput. Phys. 509 (2024) 113051.
[38] J.-P. Dalmont, C.J. Nederveen, N. Joly, Radiation impedance of tubes with different flanges: numerical and experimental investigations, J. Sound Vib. 244 (2001) 505–534.
[39] D.H. Keefe, Acoustic streaming, dimensional analysis of nonlinearities, and tone hole mutual interactions in woodwinds, J. Acoust. Soc. Am. 73 (5) (1983) 1804–1820.
[40] A. Lefebvre, G. Scavone, J. Kergomard, External tonehole interactions in woodwind instruments, Acta Acustica United Acustica 99 (2012).
[41] A. Quarteroni, A. Manzoni, F. Negri, Reduced Basis Methods for Partial Differential Equations: An Introduction, vol. 92, Springer, 2015.
[42] J.S. Hesthaven, G. Rozza, B. Stamm, et al., Certified Reduced Basis Methods for Parametrized Partial Differential Equations, vol. 590, Springer, 2016.
[43] F. Chinesta, A. Huerta, G. Rozza, K. Willcox, Ch. Model Reduction Methods, John Wiley & Sons, 2017, pp. 1–36.
[44] P. Zunino, L. Cattaneo, C.M. Colciago, An unfitted interface penalty method for the numerical approximation of contrast problems, Appl. Numer. Math. 61 (10) (2011) 1059–1076.
[45] F. de Prenter, C. Verhoosel, G. Van Zwieten, H. Van Brummelen, Condition number analysis and preconditioning of the finite cell method, Comput. Methods Appl. Mech. Engrg. 316 (2017) 297–327.
[46] P. Antolin, A. Buffa, M. Martinelli, Isogeometric analysis on v-reps: first results, Comput. Methods Appl. Mech. Engrg. 355 (2019) 976–1002.
[47] A. Logg, G.N. Wells, J. Hake, DOLFIN: A C++/Python Finite Element Library, Springer Berlin Heidelberg, Berlin, Heidelberg, 2012, pp. 173–225.
[48] P.R. Amestoy, I.S. Duff, J. Koster, J.-Y. L'Excellent, A fully asynchronous multifrontal solver using distributed dynamic scheduling, SIAM J. Matrix Anal. Appl. 23 (1) (2001) 15–41.
[49] A. Benade, Fundamentals of Musical Acoustics, Oxford U.P. New-York, 1976.
[50] P. Hennig, S. Müller, M. Kästner, Bézier extraction and adaptive refinement of truncated hierarchical NURBS, Comput. Methods Appl. Mech. Engrg. 305 (2016) 316–339.
[51] D. D'Angella, A. Reali, Efficient extraction of hierarchical B-splines for local refinement and coarsening of isogeometric analysis, Comput. Methods Appl. Mech. Engrg. 367 (2020) 113131.